Multiphoton fluorescence lifetime imaging of intrinsic fluorescence in human and rat brain tissue reveals spatially distinct NADH binding

Thomas H. Chia,[1] Anne Williamson,[2] Dennis D. Spencer,[2] and Michael J. Levene[1,*]

[1]*Department of Biomedical Engineering, Yale University, 55 Prospect St., New Haven, CT 06511, USA*
[2]*Department of Neurosurgery, Yale University, 333 Cedar St., New Haven, CT 06511, USA*
[*]*Corresponding author: Michael.Levene@yale.edu*

Abstract: Two-photon fluorescence lifetime imaging (FLIM) of molecules can reveal important information on the local microenvironment. NADH, an intrinsic fluorescent molecule and ubiquitous metabolic co-enzyme, has a lifetime that depends strongly on enzymatic binding. We present a custom image-processing algorithm for raw fluorescence lifetime and amplitude data that produces an image showing spatially distinct NADH fluorescence lifetimes in slices of rat and human brain. NADH FLIM images were collected in control and epileptic rat tissue. Differences in spatial patterns of NADH lifetimes support the hypothesis that NADH binding, and thus metabolic capacity, is significantly different between groups. This type of analysis can provide information on metabolic states in pathological material.

OCIS codes: (170.5810) Scanning Microscopy; (180.2520) Fluorescence Microscopy; (170.6935) Tissue characterization; (170.6920) Time-resolved imaging; (170.0170) Medical optics and biotechnology.

References and links

1. W. R. Zipfel, R. M. Williams, R. Christie, A. Y. Nikitin, B. T. Hyman, and W. W. Webb, "Live tissue intrinsic emission microscopy using multiphoton-excited native fluorescence and second harmonic generation," Proc. Natl. Acad. Sci. U S A **100**, 7075-7080 (2003).
2. P. Lipton, "Effects of membrane depolarization on nicotinamide nucleotide fluorescence in brain slices," Biochem. J. **136**, 999-1009 (1973).
3. K. A. Kasischke, H. D. Vishwasrao, P. J. Fisher, W. R. Zipfel, and W. W. Webb, "Neural activity triggers neuronal oxidative metabolism followed by astrocytic glycolysis," Science **305**, 99-103 (2004).
4. H. D. Vishwasrao, A. A. Heikal, K. A. Kasischke, and W. W. Webb, "Conformational dependence of intracellular NADH on metabolic state revealed by associated fluorescence anisotropy," J. Biol. Chem. **280**, 25119-25126 (2005).
5. K. Suhling, P. M. French, and D. Phillips, "Time-resolved fluorescence microscopy," Photochem. Photobiol. Sci. **4**, 13-22 (2005).
6. J. R. Lakowicz, H. Szmacinski, K. Nowaczyk, and M. L. Johnson, "Fluorescence lifetime imaging of free and protein-bound NADH," Proc. Natl. Acad. Sci. U S A **89**, 1271-1275 (1992).
7. S. J. Strickler and R. A. Berg, "Relationship between absorption intensity and fluorescence lifetime of molecules," J. Chem. Phys. **37**, 814-822 (1962).
8. L. Hertz, L. Peng, and G. A. Dienel, "Energy metabolism in astrocytes: high rate of oxidative metabolism and spatiotemporal dependence on glycolysis/glycogenolysis," J. Cereb. Blood Flow Metab. **27**, 219-249 (2007).
9. W. J. Chu, H. P. Hetherington, R. I. Kuzniecky, T. Simor, G. F. Mason, and G. A. Elgavish, "Lateralization of human temporal lobe epilepsy by 31P NMR spectroscopic imaging at 4.1 T," Neurology **51**, 472-479 (1998).
10. E. M. Cornford, M. N. Gee, B. E. Swartz, M. A. Mandelkern, W. H. Blahd, E. M. Landaw and A. V. Delgado-Escueta, "Dynamic [18F]fluorodeoxyglucose positron emission tomography and hypometabolic zones in seizures: reduced capillary influx," Ann. Neurol. **43**, 801-808 (1998).
11. H. Qu, H. Eloqayli, B. Müller, J. Aasly and U. Sonnewald, "Glial-neuronal interactions following kainate injection in rats," Neurochem. Int. **42**, 101-106 (2003).

#91453 - $15.00 USD Received 22 Jan 2008; revised 5 Mar 2008; accepted 11 Mar 2008; published 13 Mar 2008

12. T. M. Melø, A. Nehlig and U. Sonnewald, “Metabolism is normal in astrocytes in chronically epileptic rats: a (13)C NMR study of neuronal-glial interactions in a model of temporal lobe epilepsy,” J. Cereb. Blood Flow Metab. **25**, 1254-1264 (2005).
13. T. J. Ashwood, B. Lancaster and H. V. Wheal, "Intracellular electrophysiology of CA1 pyramidal neurones in slices of the kainic acid lesioned hippocampus of the rat," Exp. Brain Res. **62**, 189-198 (1986).
14. C. L. Meier and F. E. Dudek, “Spontaneous and stimulation-induced synchronized burst afterdischarges in the isolated CA1 of kainate-treated rats,” J. Neurophysiol. **76**, 2231-2239 (1996).
15. O. Kann, S. Schuchmann, K. Buchheim, and U. Heinemann, “Coupling of neuronal activity and mitochondrial metabolism as revealed by NAD(P)H fluorescence signals in organotypic hippocampal slice cultures of the rat,” Neuroscience **119**, 87-100 (2003).
16. O. Kann, R. Kovacs, M. Njunting, C. J. Behrens, J. Otahal, T. N. Lehmann, S. Gabriel, and U. Heinemann, "Metabolic dysfunction during neuronal activation in the ex vivo hippocampus from chronic epileptic rats and humans," Brain **128**, 2396-2407 (2005).
17. D. A. McCormick and A. Williamson, “Convergence and divergence of neurotransmitter action in human cerebral cortex,” Proc. Natl. Acad. Sci., U S A **86**, 8098-8102 (1989).
18. W. R. Chen, S. Lee, K. Kato, D. D. Spencer, G. M. Shepherd, and A. Williamson, “Long-term modifications of synaptic efficacy in the human inferior and middle temporal cortex,” Proc. Natl. Acad. Sci. U S A **93**, 8011-8015 (1996).
19. J. DeFelipe, “Cortical microanatomy and human brain disorders: epilepsy,” Cortex **40**, 232-233 (2004).
20. L. D. Errante, A. Williamson, D. D. Spencer, and O. A. Petroff, “Gabapentin and vigabatrin increase GABA in the human neocortical slice,” Epilepsy Res. **49**, 203-210 (2002).
21. B. N. Smith and F. E. Dudek, “Network interactions mediated by new excitatory connections between CA1 pyramidal cells in rats with kainate-induced epilepsy,” J. Neurophysiol. **87,** 1655-1658 (2002).
22. M. Tsacopoulos and P. J. Magistretti, "Metabolic coupling between glia and neurons," J. Neurosci. **16**, 877-885 (1996).
23. C. Dubé, S. Boyet, C. Marescaux, and A. Nehlig, “Progressive metabolic changes underlying the chronic reorganization of brain circuits during the silent phase of the lithium-pilocarpine model of epilepsy in the immature and adult rat,” Exp. Neurol. **162**, 146-157 (2000).
24. W. A. Gomes, F. A. Lado, N. C. de Lanerolle, K. Takahashi, C. Pan, and H. P. Hetherington, “Spectroscopic imaging of the pilocarpine model of human epilepsy suggests that early NAA reduction predicts epilepsy,” Magn. Reson. Med. **58**, 230-235 (2007).
25. S. Alvestad, J. Hammer, E. Eyjolfsson, H. Qu, O. P. Ottersen, and U. Sonnewald, “Limbic structures show altered glial-neuronal metabolism in the chronic phase of kainate induced epilepsy,” Neurochem. Res. **21,** Aug. (2007).
26. S. Pelet, M. J. R. Previte, L. H. Laiho and P. T. C. So, “A fast global fitting algorithm for fluorescence lifetime imaging microscopy based on image segmentation,” Biophys. J. **87**, 2807-2817 (2004).
27. P. R. Barber, S. M. Ameer-Beg, J. Gilbey, R. J. Edens, I. Ezike, and B. Vojnovic, “Global and pixel kinetic data analysis for FRET detection by multi-photon time-domain FLIM,” Proc. SPIE **5700,** DOI:10,1117/12.590510 (2005).

1. Introduction

1.1 NADH – Metabolic co-enzyme and intrinsic fluorophore

A powerful advantage of multiphoton microscopy is its ability to produce images in the brain using intrinsic fluorophores such as the ubiquitous co-enzyme nicotinamide adenine dinucleotide (NADH) [1]. NADH is an integral molecule in both oxidative and non-oxidative cellular metabolism. NADH loses fluorescence upon oxidation to NAD^+; thus changes in NADH fluorescence can be used to monitor metabolism in discrete cellular populations [2]. Kasischke, *et al*., (2004) [3], used multiphoton microscopy of NADH to demonstrate spatiotemporal partitioning of glycolytic and oxidative metabolism between astrocytes and neurons following stimulation. However, strict intensity measurements of NADH/NAD^+ fluorescence changes can be misleading due to differences in the fluorescence lifetime and therefore differences in quantum yield of NADH [4].

Although the fluorescence lifetime for a molecule such as NADH is constant under a characterized microenvironment, a highly metabolically active milieu such as the brain will cause variations in NADH lifetime. Vishwasrao, *et al*., [4], using fluorescence lifetime and associated anisotropy measurements, demonstrated that NADH in the rat brain exhibits multiple lifetimes. They referred to subpopulations of NADH that exhibited different lifetimes as different “species” of NADH. These species included unbound NADH in folded and extended conformations, as well as a number of NADH species bound to enzymes of varying sizes. The result was NADH lifetime measurements ranging from ~150 ps to ~6 ns.

#91453 - $15.00 USD Received 22 Jan 2008; revised 5 Mar 2008; accepted 11 Mar 2008; published 13 Mar 2008

Specific causes of lifetime variation include changes in viscosity, temperature, or pH [5], but are largely attributed to enzymatic binding. Enzymatic binding is directly related to NADH cycling through the energy production pathways. For example, one step in the citric acid cycle involves the enzyme malate dehydrogenase (MDH) and NADH:

$$\text{L-malate} + \text{NAD}^+ \xrightarrow{\textbf{MDH}} \text{oxaloacetate} + \text{NADH}$$

During this reaction, the MDH enzyme (70,000 Da) binds with NADH (633 Da), causing drastic changes in the physical behavior of NADH, in turn affecting fluorescence lifetime [6].

1.2 Fluorescence lifetime imaging of NADH

Fluorescence lifetime imaging (FLIM) is a sensitive, time-resolved technique able to measure the lifetimes of fluorescent molecules found in the image plane. Although each pixel in a FLIM image may be fit to a multiple component exponential decay, commercial FLIM software performs a weighted average at each pixel to arrive at a single effective lifetime for display and histogramming. This approach, however, can conceal important information such as changes in the distribution of distinct bound states of the fluorophore. Here we present a custom lifetime imaging program that can identify the number of unique fluorescent species in the image plane and produce a histogram showing the concentration of each species.

The amplitude (α) information carried in a FLIM image can be directly related to the fluorophore concentration irrespective of quantum efficiency. Fluorescence lifetime decay curves, F(t), are fit to a sum of exponential such that:

$$F(t) \propto \sum_i \alpha_i e^{-t/\tau_i} \tag{1}$$

The total detected fluorescence is related to the system detection efficiency (ϕ), two-photon cross-section (σ), laser intensity (I), concentration (c), and quantum efficiency (Q). This fluorescence is also equal to the summation of fluorescence lifetime multiplied by the amplitude (Eq. (2)).

$$Fluorescence = \phi\sigma I^2 \cdot c_i Q_i = \sum_i \alpha_i \int_0^\infty e^{-t/\tau_i}\, dt = \sum_i \alpha_i \tau_i \tag{2}$$

Rearranging the terms from Eq. (2) and expressing Q in terms of fluorescence and radiative lifetimes gives the expression for amplitude seen in Eq. (3).

$$\alpha_i = \frac{\phi\sigma I^2}{\tau_{radiative}} \cdot c_i \tag{3}$$

The terms ϕ and I are tested to be constant during image acquisition and σ is a physical constant. The radiative lifetime ($\tau_{radiative}$) can vary by changes in the refractive index, however, these changes are expected to be small compared to observed differences in fluorescence lifetimes [7]. In the case of NADH, previous groups have reported evidence suggesting that the radiative rate does not change significantly in tissue slices [4]. Therefore, $\alpha_i \propto c_i$ and can be used as a proxy for changes in species concentration.

We used two-photon excitation FLIM to measure differences in NADH lifetimes found in both rat hippocampus and human cortex. Astrocytes play an important metabolic role in supporting the proper function of neurons [8]. The metabolic balance between these cell types is tightly regulated and can be drastically altered in cases of neurological diseases including human temporal lobe epilepsy [9, 10]. The degree to which these metabolic changes are reproduced in the animal models remains controversial [11, 12]. We tested the metabolic

#91453 - $15.00 USD Received 22 Jan 2008; revised 5 Mar 2008; accepted 11 Mar 2008; published 13 Mar 2008

response following stimulation in control and in epileptic pilocarpine-treated rats to determine if there were differences in NADH binding and distribution that would be representative of metabolic dysfunction. In addition, we present results of this method as applied to NADH FLIM in epileptic human brain tissue

2. Materials and methods

2.1 Brain slice preparations

We used the pilocarpine-treated rat (340 mg/kg, Sprague-Dawley, Charles River) model of temporal lobe epilepsy; normal Sprague-Dawley rats served as controls. Rats were anesthetized with a pentobarbital sodium solution (50 mg/kg) and then decapitated. Their brains were rapidly removed and placed in an ice-cold cutting solution containing (in mM) sucrose, 219; $NaHCO_3$, 28; KCl, 2.5; $CaCl_2$, 0.5; $MgSO_4$, 7.0; $NaHPO_4$, 1.25; and glucose, 7 for 1-2 minutes. The brains were then blocked into a section including the hippocampus and mounted on the stage of a Vibratome (St. Louis, MO). Transverse hippocampal slices were cut 400 μm in thickness. The hippocampus was dissected free from the surrounding cortex using a scalpel. Slices were allowed to recover in oxygenated (95% O_2 / 5% CO_2) artificial cerebral spinal fluid (ACSF) for $\geq$2 hours prior to imaging. Following recovery, slices were placed into an imaging chamber (Warner Instruments, Hamden, CT) and perfused with oxygenated artificial cerebral spinal fluid (ACSF) at a rate of 0.8 mL / min using a two-channel peristaltic pump (Cole-Parmer, Vernon Hills, Illinois). The ACSF contained (in mM) NaCl, 130; KCl, 3.0; $CaCl_2$, 2.0; $MgSO_4$, 1.25; $NaHCO_3$, 28; NaH_2PO_4, 1.25 and glucose, 10.

Brain slices are generally hypometabolic compared to in vivo systems and we were concerned that differences between control and epileptic tissue would be difficult to discern at rest. Therefore, we bath applied the $GABA_A$ receptor antagonist bicuculline (30 μM) to hippocampal slices for 30 minutes. Bicuculline induces seizure-like activity (recurrent events on the order of 500 ms - 2000 ms) in tissue from pilocarpine-treated rats and shorter, more frequent events (50 ms - 200 ms duration) termed epileptiform bursts from control tissue [13, 14]**.** These types of synchronized neural activity are known to drive oxidative metabolism in vitro [15, 16].

For human tissue preparation, neocortical tissue was collected from patients undergoing resections for the treatment of medically intractable epilepsy. All patients had provided informed consent and studies were approved by the Yale University IRB. For the present study, we primarily imaged the cortex overlying epileptogenic hippocampi. This tissue is the most normal that is routinely available for live tissue studies as determined by physiological and anatomic studies [17, 18, 19] and is metabolically viable for at least 10 hours following resection [20].

The cortex was resected en bloc and a tissue slab cut orthogonal to the pia was provided. Similarly, the hippocampus was removed en bloc and transverse sections prepared. We received a section from the mid-body of the structure. The tissue was placed in ice-cold cutting solution and rapidly transported to the laboratory where slices were prepared as above. The time between resection and slicing was approximately 10 minutes. The imaging and analysis was identical to the rat material.

2.2 Microscope apparatus

We used a custom-built multiphoton microscope based on an Olympus BX51 WI upright fluorescence microscope (Olympus America, Center Valley, PA). The excitation source was an 80 MHz pulsed Ti:Sapphire (Ti:S) laser (Mai Tai, Spectra-Physics, Mountain View, CA) tunable between 710 nm and 990 nm. Unless otherwise noted, excitation was at 769 nm with a 100 fs pulsewidth. The microscope objective was a 20x/0.95 NA water immersion objective (Olympus, XLUMPLFL). Samples were placed on a motorized 3-axis microscope stage (ASI Imaging, Eugene, OR).

FLIM capabilities were made possible through the addition of a multi-channel plate PMT (R3809U-52, Hamamatsu) and a time-correlated single photon counting (TCSPC) card (SPC-

#91453 - $15.00 USD Received 22 Jan 2008; revised 5 Mar 2008; accepted 11 Mar 2008; published 13 Mar 2008

150, Becker & Hickl, Berlin, Germany). NADH fluorescence was filtered through a 555 nm short-pass filter (Chroma Technologies, Rockingham, VT). Images were acquired by summation of 50, 0.8-second scans. Fluorescence decay curves in image pixels were processed using SPC Image (Becker & Hickl). The software was able to calculate the basic fluorescence lifetimes on a pixel-by-pixel basis and account for the instrument response function (IRF). For every pixel in the image, the eight nearest-neighbor pixels relative to each central pixel were binned together to increase photon counts for improved decay fits. Typical signal levels after binning were roughly 1200 photons per pixel. All fluorescence lifetimes were fit using SPC Image (Becker & Hickl). Typical χ^2 values obtained from fitting lifetime images to one-, two-, and three-component fits are shown in Fig. 1. All NADH lifetime calculations were fit to two-components, as determined by obtaining the lowest χ^2 fit value (Fig. 1(b)). A fluorescent slide was used to confirm uniform illumination intensity throughout the image plane and laser power was kept well below saturation levels.

The full width at half maximum (FWHM) of the IRF was 62 ps as measured from the second-harmonic generation of rat-tail collagen. The accuracy of the system was verified by measuring the lifetime of a known standard (unbound NADH in solution). NADH fluorescence decay measurements for these validation experiments were also fit to a two-component decay; unbound NADH in solution exists in two molecular conformations [4]. Our amplitude-weighted average lifetime result of 480 ps was in good agreement with a 444 ps lifetime measurement obtained by a previous group [4]. In addition, we have added the enzyme, malate dehydrogenase (MDH) to a solution of unbound NADH. The lifetime increased from 480 ps to 769 ps. This showed that MDH (non-fluorescent) was binding to NADH (fluorescent) and thereby increasing its fluorescence lifetime.

2.3 Image processing

The algorithm we have developed takes a fluorescence lifetime image in which each pixel has been fit to multiple components. The raw data matrices (256 x 256 pixels or elements) from the fits ($amplitude_1$, $amplitude_2$, etc., and $lifetime_1$, $lifetime_2$, etc.) are imported into the custom program. The program generates a histogram of fluorescence lifetimes present in the image. However, instead of recording a single, amplitude-weighted average lifetime from each pixel (as is commonly done in commercial software), each component of each pixel is counted into the histogram weighted by its amplitude. For a lifetime image composed of two-component fits, each pixel thereby contributes two separate lifetimes to the histogram, weighted by their respective fit amplitudes (Fig. 2). The resulting histogram can clearly indicate multiple, unique fluorescence lifetimes found throughout the image without any lifetime averaging. The user is then prompted to define the boundary point between each lifetime peak and assign a corresponding color for each lifetime peak. This allows a color-coded image to be created indicating the spatial location of molecules represented by the peaks found in the lifetime histogram. The custom FLIM analysis program can be made available to any labs that contact the corresponding author.

Between 5-7 non-overlapping images were taken before and after bicuculline stimulation for control and pilocarpine-treated tissue. This resulted in a total of 24 lifetime images analyzed to calculate NADH concentration measurements from all treatment groups. All images were acquired from the CA1 region of the hippocampus and images from before and after bicuculline simulation were taken from the same regions of interest. For this methodological study, we examined slices from one age-matched control and one epileptic, pilocarpine-treated animal. In the absence of electrophysiological recordings, slices from only one animal type were used to limit variability in patterns and degrees of excitation [21].

#91453 - $15.00 USD Received 22 Jan 2008; revised 5 Mar 2008; accepted 11 Mar 2008; published 13 Mar 2008

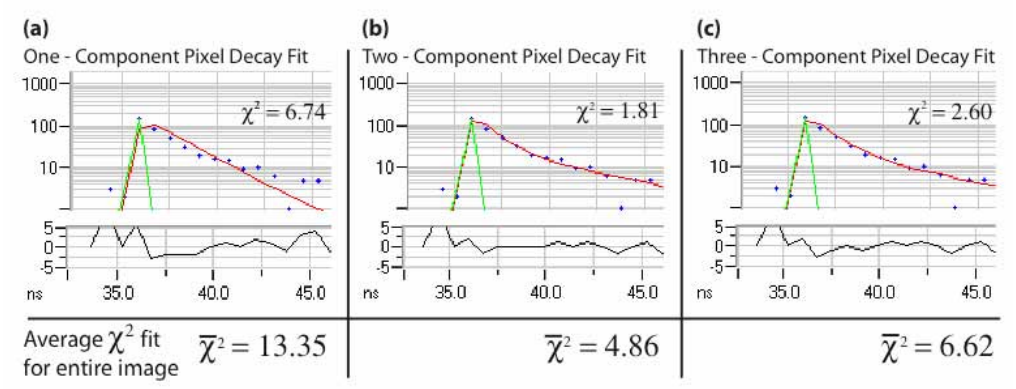

Fig. 1. The top row of the figure are sample NADH fluorescence lifetime decay fit curves (red line) for the same, individual pixel given a one- (a), two- (b), and three- (c) component fit. The calculated χ^2 value for the pixel is provided, green line is the instrument response function, and blue dots are delayed photon counts arriving after the laser excitation pulse. The bottom row is the average χ^2 value averaged from all the pixels in the image. The minimal χ^2 value is achieved with a two-component fit (b). The χ^2 value for a three-component fit increases due to increasing the number of fit parameters without significantly increasing the quality-of-fit.

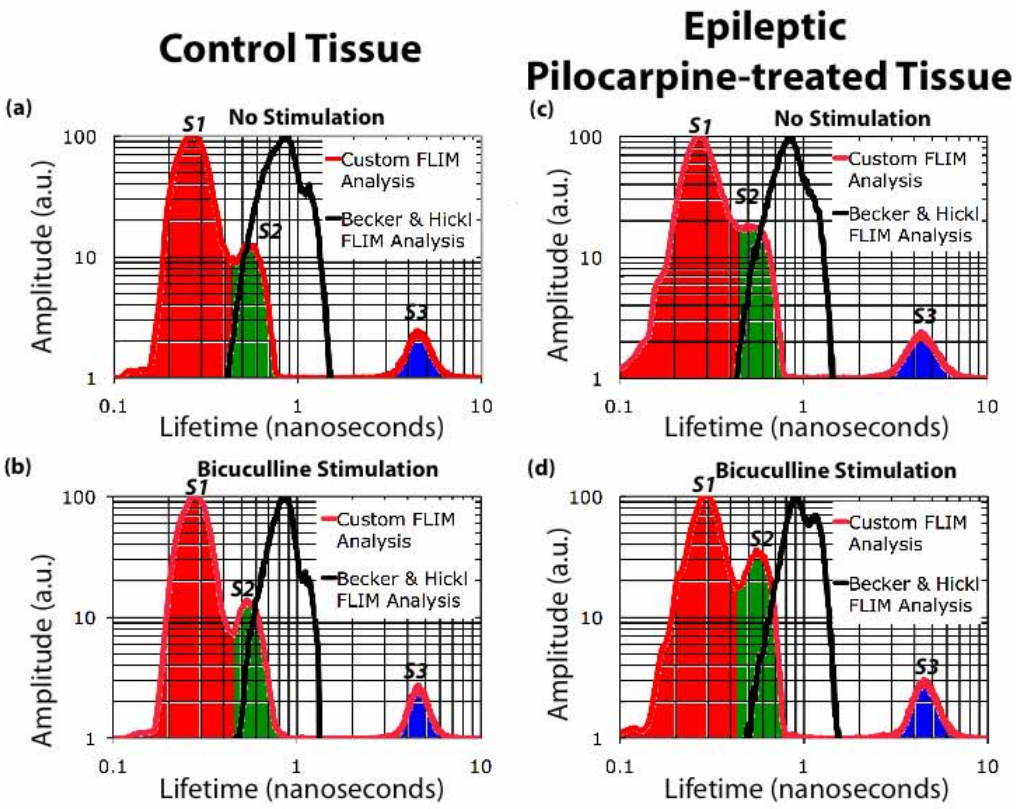

Fig. 2. (a). (c) Sample distribution of NADH lifetimes seen in the control and pilocarpine-treated rat hippocampus before bicuculline stimulation. Red line shows the NADH lifetime distribution obtained with the custom program. Three distinct NADH species are clearly identified: unbound NADH (red / S1) and two bound NADH species (green / S2 and blue / S3). Black line is the NADH distribution obtained from the Becker & Hickl FLIM analysis program where a single, amplitude-weighted average lifetime is obtained from each pixel. (b), (d) Sample NADH lifetime distributions obtained using the custom program and the Becker & Hickl program following bicuculline stimulation in control and pilocarpine-treated tissue, respectively.

#91453 - $15.00 USD Received 22 Jan 2008; revised 5 Mar 2008; accepted 11 Mar 2008; published 13 Mar 2008

3. Results

3.1 Histogram data

One-, two-, and three-component fits to lifetime decays were compared. The bottom row of Fig. 1 shows the mean χ^2 value obtained when χ^2 values in every image pixel are averaged together. The two-component fit achieved the best χ^2 for the NADH lifetime images. A three-component fit resulted in an increase in χ^2 due to increasing the number of fit parameters without substantially increasing the quality of fit. In addition, the histogram produced using a three-component fit reveals a peak of NADH lifetimes between 6.2 ns – 12 ns, a time scale that is large compared to the integration time and is therefore likely artifactual. In addition, NADH fluorescence lifetimes in this range were not found by Vishwasarao [4]. After processing the raw rat hippocampus and human cortex lifetime data using our custom program, at least three distinct lifetime peaks were observed (Fig. 2). The peak with greatest amplitude and a narrow line-width typically occurred around 200 ps - 450 ps (species #1). A second peak with medium amplitude and a narrow line-width occurred around 450 ps - 800 ps (species #2). Finally, a peak with small amplitude and broad line-width appeared at lifetimes ranging from 3 ns - 6 ns (species #3). The shortest lifetime peak corresponds to unbound NADH while the two longer lifetime peaks correspond to bound NADH [4].

It is important to note that fluorescent molecules with long lifetimes contribute more to fluorescence intensity images due to their greater quantum yield (or effective brightness). FLIM possesses the ability to measure the concentration of fluorescent molecules regardless of their quantum yields. This custom algorithm helped interpret NADH concentration in the sample by plotting the histogram weighted by amplitude (directly related to concentration). Therefore, based on Fig. 2, species #1 is present in the greatest concentration. Species #3 has the longest lifetime and greatest brightness, but is typically the least concentrated.

In the case of the pilocarpine-treated, epilepsy model rat, the middle peak (species #2) was suppressed (Fig. 2(c)) compared to untreated animals. Upon application of bicuculline, the middle lifetime peak appeared, creating a lifetime histogram similar to a control rat (Fig. 2(d)). The other two peaks remained relatively unchanged following the application of bicuculline. Figure 2 also compares the custom lifetime histogram to the histogram produced by the Becker & Hickl SPCImage program using a single, amplitude-weighted average lifetime for each pixel. Note how in the Becker & Hickl method, the longest lifetimes (blue) averaged with the shorter lifetimes to yield a distribution of lifetimes not actually present in the sample.

The amplitude of each peak in the histogram provides the concentration of NADH. Figure 3 shows the concentration (a.u.) and concentration changes of each NADH species following bicuculline stimulation for the cell layer and dendritic layer. The cell and dendritic layer are analyzed separately in each image because of the distinct energetic differences between these regions. The bulk of excitatory synapses are made on the dendrites and are surrounded by glial processes. In contrast, there are fewer synaptic contacts in the cell layer and a looser glial wrap. Therefore we expect greater NADH changes in the dendritic versus the somatic compartments, especially under activated conditions. In both the control rat and the pilocarpine-treated rat, the NADH concentration increased as expected. However, there are significant differences in the concentrations and the degree of NADH concentration changes between these two groups. The concentrations of species #1 and #2 differ markedly between control and epileptic tissue both with and without stimulation.

#91453 - $15.00 USD Received 22 Jan 2008; revised 5 Mar 2008; accepted 11 Mar 2008; published 13 Mar 2008

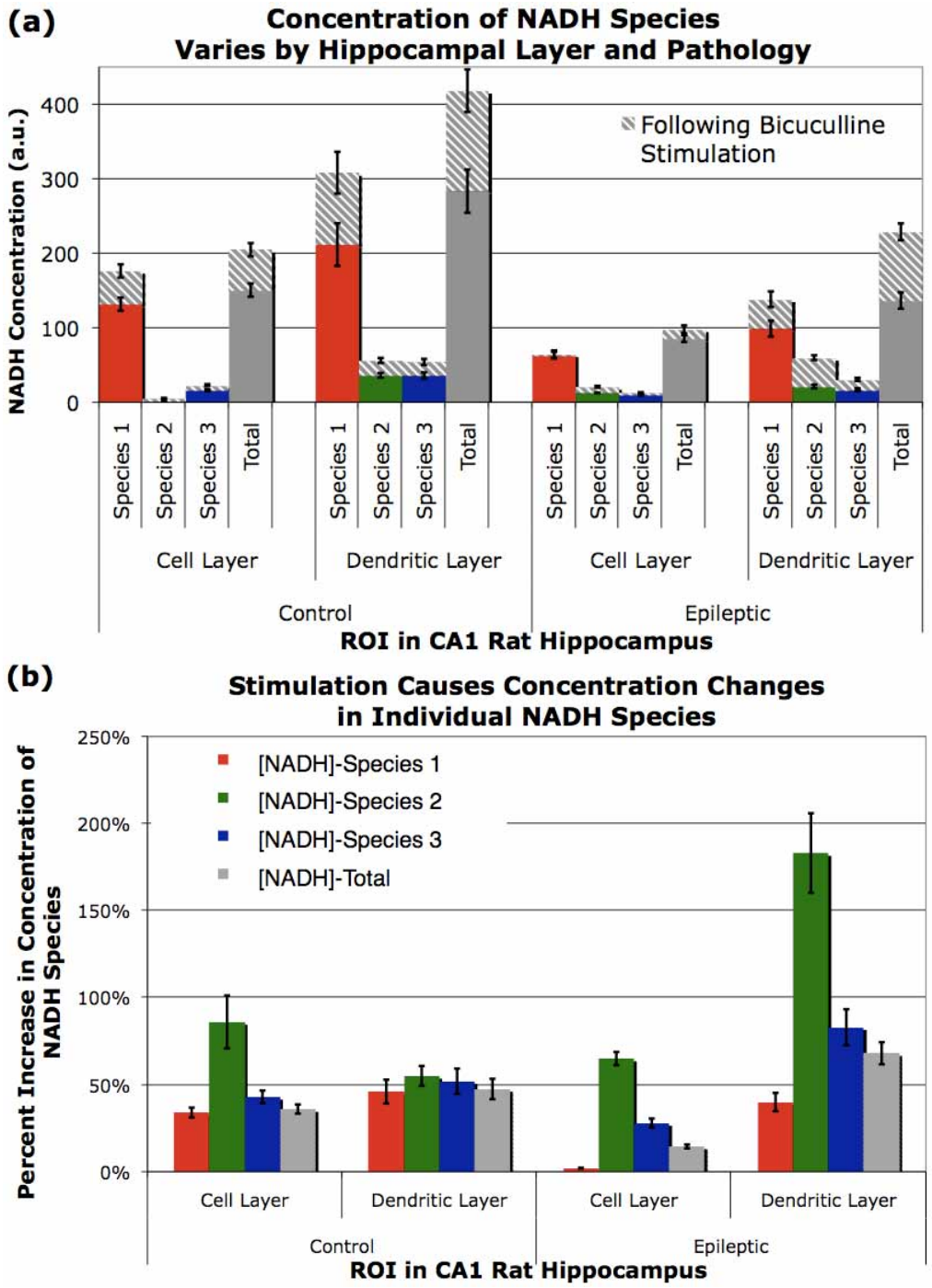

Fig. 3. (a). Concentration of NADH species varies across brain region and following bicuculline stimulation. There is a large difference in concentration between species #1 and #2 in all cases. (b) Concentration increases of each NADH species following bicuculline stimulation in the CA1 rat hippocampus. Notice the significant changes species #2 in the dendritic layer of the pilocarpine-treated rat.

#91453 - $15.00 USD Received 22 Jan 2008; revised 5 Mar 2008; accepted 11 Mar 2008; published 13 Mar 2008

3.2 Image processing data

The second-half of the program analyzes the spatial distribution of these distinct NADH lifetimes to help elucidate the physiological significance behind the amplitude changes. Figure 4(a), shows the NADH autofluorescence intensity image from which the pilocarpine-treated lifetime histogram in Fig. 2 is taken. The arrows in Fig. 4(a) point to astrocytes near the cell layer (C.L.) in the CA1 region of the hippocampus. Astrocytes can be distinguished in NADH fluorescence intensity images by their elevated cytosolic fluorescence signal relative to the background. In contrast, neurons display less cytosolic fluorescence, but are characterized by bright, punctate spots where NADH is concentrated in the mitochondria [22]. Figures 4(b) and 4(c) present the Becker & Hickl color-coded FLIM image and its respective lifetime histogram.

When the custom FLIM image was decomposed into its separate red, green, and blue color channels (Fig. 5), interesting information regarding NADH binding was revealed. The unbound NADH (red) and long lifetime NADH (blue) appear higher in cell bodies in their distribution and are co-localized with the astrocytes in Fig. 4(a). The shorter lifetime bound NADH (green) has no cellular resemblance and corresponded exclusively to the neuropil. The neuropil is predominately composed of neuronal and astrocytic processes and is the site for most synaptic contacts. Note that species #1 (red) and #2 (green) are mutually exclusive pixels (Fig. 5(d). Although this may at first appear to be an artifact of fitting to bi-exponentials, fits to three lifetimes do not result in images in which species #1 and #2 co-localize; rather, as stated above, a longer and likely artifactual lifetime results that does not improve the overall quality of fit.

Higher magnification images of neurons in the human cortex and astrocytes in the rat hippocampus revealed more detailed information about the intracellular NADH distribution. Figure 6 clearly shows that the long lifetime NADH (blue) is most concentrated within the mitochondria of the cells and the unbound NADH (red) is primarily cytosolic.

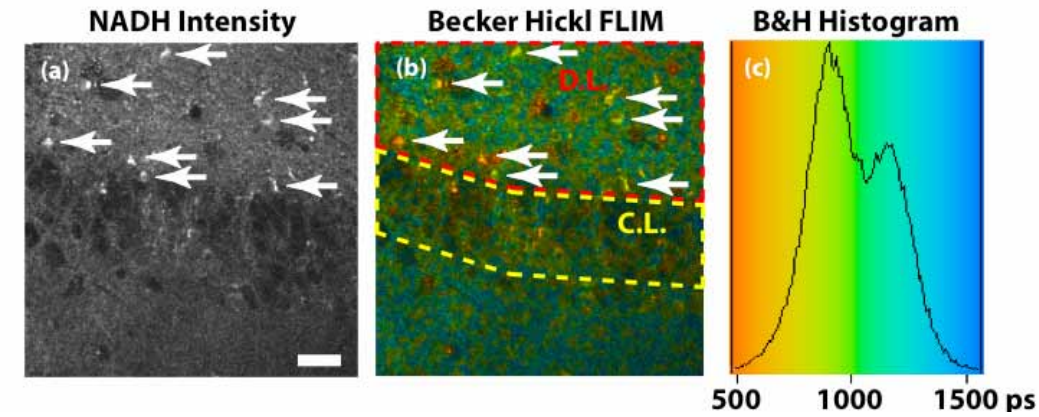

Fig. 4. Intensity (a) and Becker & Hickl FLIM (b) images generated using NADH autofluorescence in the pilocarpine-treated rat hippocampus (with bicuculline stimulation). Arrows in (a) point to astrocytes in the dendritic layer (D.L). Cell layer (C.L.) appears dark due to absence of NADH in the nuclei. The D.L. is bounded by a red, dotted line and the C.L. is bounded by a yellow, dotted line. NADH lifetimes in (b) correspond to the Becker & Hickl color histogram (c). Scale bar = 20 µm.

#91453 - $15.00 USD Received 22 Jan 2008; revised 5 Mar 2008; accepted 11 Mar 2008; published 13 Mar 2008

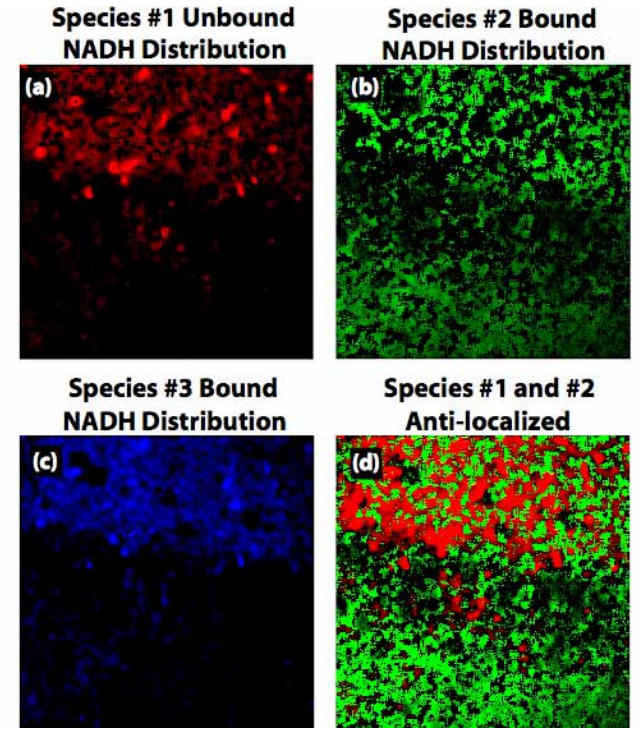

Fig. 5. Custom FLIM images generated from the histogram data used in Fig. 2 (pilocarpine-treated rat hippocampus). Custom FLIM image are separated into images that correspond to the color-coded lifetime shown in Fig. 2. Note how unbound NADH (a, red, ~300 ps) and heavily bound NADH (c, blue, ~4500 ps) appear with more cellular morphology, whereas lightly bound NADH (b, green, ~560 ps) is localized to the neuropil. Part (d) is a saturated, merged image of (a) and (b) to show the anti-localization of these two NADH species. Scale bar = 20 μm.

#91453 - $15.00 USD Received 22 Jan 2008; revised 5 Mar 2008; accepted 11 Mar 2008; published 13 Mar 2008

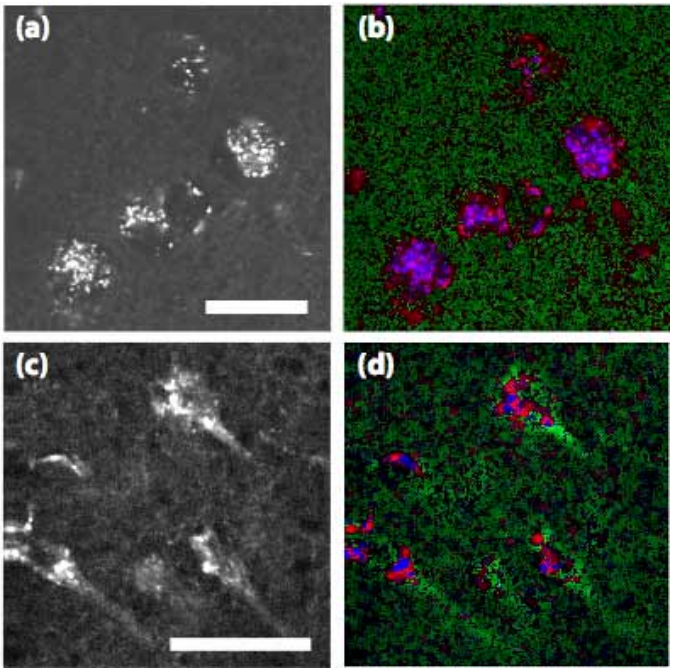

Fig. 6. Close-up intensity (a,c) and custom FLIM (b,d) images generated using NADH autofluorescence in the human cortex (a,b) and rat hippocampus (c,d), clearly showing neurons. The bright, punctate spots are NADH-rich mitochondria. Custom FLIM image reveals the intracellular composition of NADH: mitochondria contain primarily long lifetime NADH (blue, 3000 ps - 6000 ps) and unbound NADH (red, ~300 ps) is localized in the cytoplasm. Neuropil is composed largely of small-enzyme bound NADH (green, ~560 ps). Scale bar = 20 μm.

4. Discussion

4.1 NADH concentration in control rat and epileptic pilocarpine-treated rat

It is expected that metabolic differences between control tissue and pilocarpine-treated tissue would be evident in response to the increased neural activation produced by bicuculline stimulation. Kann, *et al*., (2005) showed these two groups had differences in bi-phasic NADH fluorescence dynamics following focal electrical stimulation. From their results, they hypothesized that altered metabolism in the epileptic brain tissue may stem from defects in the mitochondria, astrocytic glycolysis, and/or neuronal-astrocytic coupling [15]. However, examining NADH fluorescence intensity changes alone can be misleading due to differences in quantum efficiency. Our method of image processing examines changes in NADH concentration irrespective of quantum efficiency. In addition this method identifies NADH in different binding states and their spatial location in the image plane. Therefore, this custom technique can remove artifacts that would drastically affect the interpretation of NADH fluorescence changes.

Using a two-component decay fit, we identified at least three unique NADH lifetimes in the rat and human brain. The data in Fig. 3(a) suggests that NADH concentrations are lower under resting condition for the pilocarpine-treated tissue compared to the control tissue. An overall reduced NADH concentration in the pilocarpine-treated rat could be expected given a reduced metabolic potential of the neurons and astrocytes or an overall loss of neurons (a hallmark of epilepsy). However, images from control tissue and pilocarpine-treated tissue were acquired on separate days, and more precise calibration of laser intensity and system efficiency from day-to-day would be required to rule out artifacts in the observed differences in total fluorescence. Nonetheless, relative concentration comparisons of each species within each tissue group are valid and offer insight into the binding states of NADH.

#91453 - $15.00 USD Received 22 Jan 2008; revised 5 Mar 2008; accepted 11 Mar 2008; published 13 Mar 2008

In all cases, the total concentration of NADH rises in response to stimulation, as expected. For the control rat, the total NADH concentration increase is fairly uniform between the cell and dendritic layers. There is a larger increase in the medium-lifetime component in the cell layer, however, the other components do not differ significantly from each other. The increase is uniform across all species in the dendritic layer. This indicates that the distribution of NADH between free and bound species remains unchanged in the dendritic layer, and shifts in favor of a bound species in the cell layer.

In contrast, tissue from pilocarpine-treated rat demonstrates significant redistribution of NADH species in response to stimulation. There is a marked rise in species #2 in the dendritic layer, and almost no change in unbound NADH concentration in the cell layer. While the total NADH concentration rises more in the dendritic layer compared to control tissue, the cell layer from pilocarpine-treated rats shows a smaller change compared to either control rats or the dendritic layer of pilocarpine-treated rats. The differences in NADH distribution in response to stimulation may be indicative of metabolic dysfunction that reflects the accumulation of NADH, suggestive of a decreased oxidative metabolism in this tissue. Moreover, this effect is greatest in the dendritic layer where the bulk of the activated synapses are found (Fig. 3). Thus, these data provide convincing evidence that there are profound changes in oxidative metabolism in this model that have been missed by other techniques [10, 11, 23]; however see [24, 25].

These changes in NADH concentration and distribution in response to stimulation would be difficult, if not impossible, to discern with the traditional amplitude-weighted averaging approach (e.g. Fig. 2, black line) which averages out the longest lifetime species (3000 ps - 6000 ps) with the shorter NADH lifetimes (100 ps - 800 ps). This processing method smears out differences from pixel to pixel. For example, two different pixels under an amplitude-weighted, averaging scheme may both arrive at a single lifetime of 1.65 ns. Yet one pixel may posses 80% of a 0.6 ns lifetime species and 20% of a 6.0 ns lifetime species, while the other pixel comprises of 50% of a 0.3 ns lifetime species and 50% of a 3.0 ns lifetime species. These pixels would result in the same color-coding in an amplitude-weighted averaging algorithm, when the true lifetime composition of these pixels is radically different. In addition, our custom lifetime histogram method avoids changing the single, averaged lifetime value when only one fluorescent species is changing lifetime in response to stimulation. The custom histogram allows individual lifetime species to change lifetimes and amplitudes without any effect on the lifetime values of other fluorescent species also found in that pixel.

4.2 Spatial segregation of NADH species

Detailed images of neurons and astrocytes in the human cortex and rat hippocampus (Fig. 6) show clear segregation in NADH species. The bright, punctate spots inside the cells are the result of concentrated NADH in the mitochondria [3]; this is also where we find the highest concentration of the longest lifetime NADH species. This is as expected given the metabolically active nature of the mitochondria. Without associated anisotropy information, it is difficult to determine whether this long lifetime is due to enzymatic binding or another microenvironmental condition (e.g. changes in viscosity). However, Vishwasrao, *et al*., (2005) found an ~6 ns NADH species in the rat brain which matched well with anisotropy information linking it to enzymatic binding. This is corroborated by the fact that NADH engages with multiple enzymes during oxidative metabolism inside the mitochondria. Overall, the degree of NADH binding is expected to correlate with local enzymatic and metabolic load. The shorter-lifetime bound NADH (green) is found in the neuropil, which is expected since the bulk of dendritic synapses are primarily located in the neuropil and have greater metabolic demand than the cytosolic compartment of the cell (unbound NADH). A concern for these studies is that we do not know the physiological state of the tissue during image acquisition. However, this concern is partially obviated by the long collection times that result in temporal averaging of neural activity at the imaging site. Future studies will attempt to link measured NADH lifetimes to identified physiological conditions (e.g. at rest vs. epileptiform activity).

#91453 - $15.00 USD Received 22 Jan 2008; revised 5 Mar 2008; accepted 11 Mar 2008; published 13 Mar 2008

5. Conclusion

Fluorescence lifetime imaging (FLIM) and two-photon imaging are both growing, and complementary, techniques for elucidating neural function. However, properly mating these techniques together in complicated biological systems is not always straightforward due to enzymatic binding, local viscosity differences, temperature, or pH changes in a biological milieu. As a result, it is important to correctly quantify the specific lifetimes in the sample as it may reveal important metabolic and functional information.

It is possible in many commercial FLIM analysis software programs to fit each pixel's fluorescence decay curve to 1, 2 or 3+ components. However, it is entirely possible that each fluorescence decay curve fits best to only a few components, but that a larger variety of fluorescent lifetimes may be exhibited throughout the sample. In addition, FLIM programs typically average the multiple lifetimes in each pixel, weighted by amplitude, and present a continuous color-coded histogram for the image. Although this approach may be appropriate in certain situations, it can create the illusion of a wide range of fluorescent lifetimes when in fact there are only a discrete number of unique fluorescent species.

Many fluorophores, both intrinsic and extrinsic, can exhibit multiple lifetimes and can change lifetimes depending on the local microenvironment. It is important to accurately segregate these species and calculate the relative contribution of each species in every pixel. We have presented a novel method to properly quantify and visualize multiple fluorescent species and have applied this program to analyze metabolic differences in control versus epileptic brain tissue. Furthermore, our technique was successfully applied to intrinsic NADH imaging in living human brain tissue. The results of our approach may also be used as a basis for image segmentation and derivation of assumed lifetimes for global analyses, which can enhance the resolution of lifetime values with low-photon counts [26, 27]. However, for our purposes, the resolution of lifetime values was sufficient to identify the distribution of major NADH species in the metabolic pathway. We predict this type of analysis will become increasingly more important as researchers use FLIM to address dysfunctional cellular metabolism in both the human and in animal models of human neurologic disease.

Acknowledgments

We thank Joseph P. Zinter for his technical assistance on the multiphoton microscope instrumentation. This work is supported by the Dana Foundation to MJL and NIH grant NS054038 to DDS and AW.

#91453 - $15.00 USD Received 22 Jan 2008; revised 5 Mar 2008; accepted 11 Mar 2008; published 13 Mar 2008